CREEP FORCE ESTIMATION AT THE WHEEL-RAIL INTERFACE

Christopher Ward, Roger Goodall and Roger Dixon
Control Systems Group, School of Electronic, Electrical and Systems Engineering, Loughborough University
Loughborough, Leicestershire, UK, LE11 3TU
e-mail: c.p.ward@lboro.ac.uk

Abstract

The railway industry in the UK is currently expanding the use of condition monitoring of railway vehicles. These systems can be used to improve maintenance procedures or could potentially be used to monitor current vehicle running conditions without the use of cost prohibitive sensors. This paper looks at a proposed method for the online estimation of creep forces in the wheel/rail contact that utilises a set of modest cost sensors and Kalman-Bucy filtering. Interpretation of these creep forces could be used for many applications but in particular the detection of areas of low adhesion.

1. INTRODUCTION

The railway industry in the UK is currently taking formative steps in the use of real time condition monitoring of railway vehicles, [1]. Monitoring can either be used to improve the maintenance procedures for railway vehicles, or used to determine current running conditions of in service vehicles without the use of cost prohibitive sensors. The study presented here is concerned with the latter class and its primary aim is the estimation of creep forces of the wheel/rail contact, previously highlighted in [2]. Estimation of these parameters has many applications, such as: local adhesion level estimation; prediction of rolling contact fatigue; prediction of wheel tread wear; estimation of track damage caused by specific vehicles; and potentially as a cost effective method of assessing engineering design changes to wheel tread geometry. The basic principles of the technique are: use of modest cost inertial sensors mounted on the body, bogie and the wheelsets; and advanced model based filtering of the signals producing 'real-time' estimates. This paper focuses upon a comparison from a vehicle dynamics viewpoint of the force estimation results arising from the estimation technique highlighted in [3].

2. SYSTEM MODELLING

The aim of the process is to determine the creep forces present in the wheel/rail contact as a rail vehicle is operating in normal traffic. As in previous studies the simulation model used here is considered only in a lateral and yaw sense as the vertical and longitudinal effects can be neglected [4]. The model can be thought of in two sections: the wheel/rail contact where the complex non-linear interactions occur; and the Newtonian mechanics of the specific vehicle's suspension systems and associated geometries.

This study is concerned with assessing the effects of varying adhesion conditions in the wheel/rail contact, therefore use is made of the contact force model developed by Polach [5]. This curve fitting mechanism can include the assumption that the initial creep curve has a varying slope for different adhesion conditions, which is not the case in Kalker theory [6]; such a characteristic has been shown experimentally in [7] and is currently being verified by a partner project taking place at the University of Sheffield using an experimental roller rig. Using this method the creep force (excluding spin effects) is calculated as

$$F = \frac{2Q\mu}{\pi}\left(\frac{k_A\varepsilon}{1+(k_A\varepsilon)^2} + \arctan(k_S\varepsilon)\right), \quad k_S \le k_A \le 1 \tag{1}$$

where k_A in the area of adhesion and k_S is the area of slip, Q is the wheel load, and ε is the gradient of the tangential stress in area of adhesion. The friction coefficients rely upon the slip velocity as

$$\mu = \mu_0 \left[(1 - A) e^{-Bw} + A \right] \tag{2}$$

where w is the total slip velocity, A is the ratio of limit friction coefficient at infinity slip velocity μ_∞ to the maximum friction coefficient μ_0, and B is the coefficient of exponential friction decrease.

Therefore specific adhesion conditions are set by five key parameters, see Table 1 in the Appendix. Where, for this study different levels of adhesion are set as: dry; wet; low; and very low. The accompanying creep curves for 20 m/s vehicle velocity are shown in Figure 1. This shows the variation in the initial slope of the creep curve and how this reduces with a reduction in the adhesion level.

In simulation these different adhesion conditions give distinct differences in terms of creep forces generated, meaning characteristics such as low adhesion can potentially be detected. Figure 2 shows the effect of a reduction of adhesion on the time history of a lateral creep force for the same lateral track irregularity. This again shows that as the adhesion level in the contact reduces the accompanying creep forces generated also reduce.

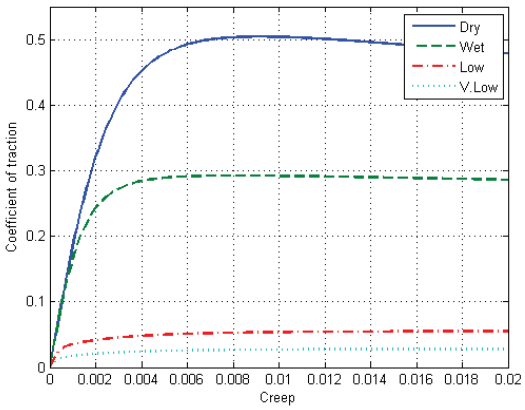

Figure 1 Varying adhesion creep curves

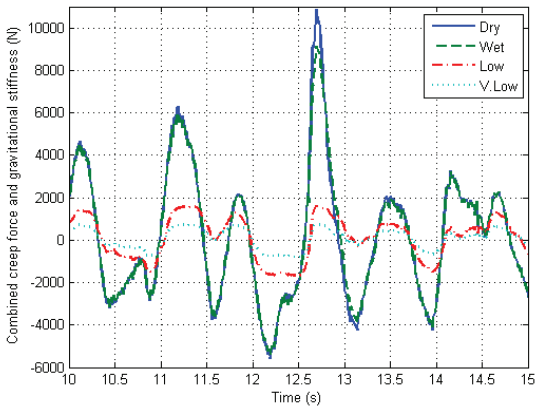

Figure 2 Simulation creep force variation

Previous studies [2] modelled the system as a half vehicle body constrained in yaw, with one bogie and two wheelsets. The model is extended here to a full vehicle body, with two bogies and four wheelsets. These equations encompass the lateral and yaw dynamics of the wheelsets, the bogies and the vehicle body. Dynamic equations adapted for the Newtonian vehicle dynamics from [8] are given below. The dynamics of each leading wheelset in a bogie is given for the lateral dynamics as (shown here for the front bogie)

$$m_W \ddot{y}_{FF} = F_{LyFF} + F_{RyFF} + F_{gFF} + F_{syFF} \tag{3}$$

with the accompanying yaw dynamics as

$$I_W \ddot{\psi}_{FF} = F_{LyFF} R_{LxFF} - F_{LxFF} R_{LyFF} + F_{RyFF} R_{RxFF} - F_{RxFF} R_{RyFF} + M_{gFF} + M_{s\psi FF} \tag{4}$$

The dynamic equations of the trailing wheelset lateral dynamics are

$$m_W \ddot{y}_{FR} = F_{LyFR} + F_{RyFR} + F_{gFR} + F_{syFR} \tag{5}$$

with the yaw dynamics as

$$I_W \ddot{\psi}_{FR} = F_{LyFR} R_{LxFR} - F_{LxFR} R_{LyFR} + F_{RyFR} R_{RxFR} - F_{RxFR} R_{RyFR} + M_{gFR} + M_{s\psi FR} \tag{6}$$

The leading bogie lateral dynamics are

$$m_B \ddot{y}_{BF} = -\left(F_{syFF} + F_{syFR} + F_{syVF} \right) \tag{7}$$

with the accompanying yaw dynamics

$$I_B \ddot{\psi}_{BF} = -\left(M_{s\psi FF} + M_{s\psi FR} + M_{s\psi VF} \right) - L\left(F_{syFF} - F_{syFR} \right) \tag{8}$$

The trailing bogie lateral dynamics are

$$m_{BR} \ddot{y}_{BR} = -\left(F_{syRF} + F_{syRF} + F_{syVR} \right) \tag{9}$$

with the accompanying yaw dynamics

$$I_{BR}\ddot{\psi}_{BR} = -\left(M_{s\psi RF} + M_{s\psi RR} + M_{s\psi VF}\right) - L\left(F_{syRF} + F_{syRR}\right) \tag{10}$$

The full length vehicle body lateral dynamic equations

$$m_V \ddot{y}_V = F_{syVF} + F_{syVR} \tag{11}$$

with the accompanying yaw dynamics

$$I_V \ddot{\psi}_V = M_{s\psi VF} + M_{s\psi VR} \tag{12}$$

where F_{ijkl}, R_{ijkl} , M_{ijkl} are the forces (creep, gravitational and suspension), positions and moments, m_{kl} is the mass, I_{kl} is the moment of inertia, y_{kl} is the lateral position, ψ_{kl} is the yaw angle; where *i=L(eft), R(ight), s(uspension)*; *j=x(longitudinal), y(lateral)*; *k=F(ront bogie), R(ear bogie), V(ehicle)*; *l=F(ront wheelset), R(ear wheelset), B(ogie)*. The current candidate vehicle for future testing is a British Rail Mk.3 coach, as this type of vehicle is readily available and is part of the New Measurement Train (NMT) where full scale application may occur. The layouts of the primary and secondary suspensions are shown if Figures 3 and 4 respectively, with constants used in Table 2 in the Appendix.

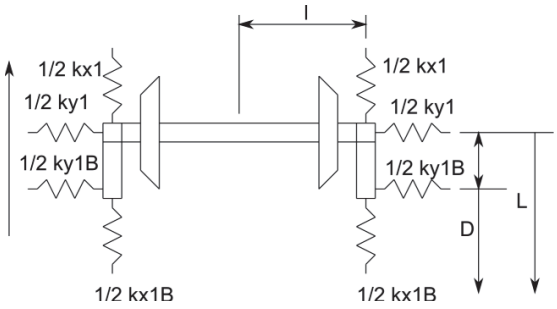

Figure 3 Primary suspension geometry

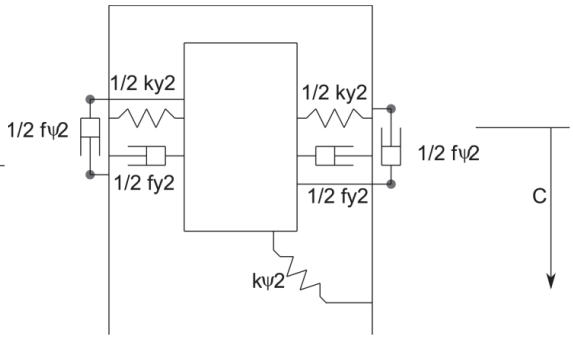

Figure 4 Secondary suspension geometry

3. CREEP FORCE ESTIMATION TECHNIQUE

The well known Kalman-Bucy filter [9] is used to estimate the creep forces, combined with the gravitational stiffness. Previous studies showed [10] that the Kalman filter as set up cannot distinguish between the creep forces and the gravitational stiffness so these need to be combined in the estimation. Therefore in the estimation filter the dynamic equations for the wheelsets of the leading bogie equations 3 to 6 become

$$m_W \ddot{y}_{FF} = F_{FF} + F_{syFF} \tag{13}$$

$$I_W \ddot{\psi}_{FF} = M_{FF} + M_{s\psi FF} \tag{14}$$

$$m_W \ddot{y}_{FR} = F_{FR} + F_{syFR} \tag{15}$$

$$I_W \ddot{\psi}_{FR} = M_{FR} + M_{s\psi FR} \tag{16}$$

Where for the trailing bogie the equivalent equations are

$$m_W \ddot{y}_{RF} = F_{RF} + F_{syRF} \tag{17}$$

$$I_W \ddot{\psi}_{RF} = M_{RF} + M_{s\psi RF} \tag{18}$$

$$m_W \ddot{y}_{RR} = F_{RR} + F_{syRR} \tag{19}$$

$$I_W \ddot{\psi}_{RR} = M_{RR} + M_{s\psi RR} \tag{20}$$

Where for the filter to operate the following assumptions are made

$$\dot{F}_{FF} = \dot{F}_{FR} = \dot{F}_{RF} = \dot{F}_{RR} = 0 \tag{21}$$

$$\dot{M}_{FF} = \dot{M}_{FR} = \dot{M}_{RF} = \dot{M}_{RR} = 0 \tag{22}$$

In this system, the design model is chosen such that the system input (track irregularity) is not included, and the filter becomes output only as it only uses measurements from the rail vehicle, therefore $C_k = D_k = 0$. Further studies have looked into the sensing requirements for the method, and some brief conclusions are that: only half the vehicle needs to be instrumented; no measurements are required on the vehicle body; and measurements are required either side of the primary suspension in the axle-box and on the bogie. The example outputs shown below are for an estimation model applied to signals generated from the front half of the simulation model, with a full measurement set for the two wheelsets, the bogie and the lateral dynamics of the vehicle body. The state vector for the estimation model is therefore defined as

$$x = \left[y_{FF}\ \dot{y}_{FF}\ \psi_{FF}\ \dot{\psi}_{FF}\ y_{FR}\ \dot{y}_{FR}\ \psi_{FR}\ \dot{\psi}_{FR}\ y_{BF}\ \dot{y}_{BF}\ \psi_{BF}\ \dot{\psi}_{BF}\ \cdots \right.$$
$$\left. y_V\ \dot{y}_V\ F_{FF}\ F_{FR}\ M_{FF}\ M_{FR} \right]^T \tag{23}$$

with the corresponding output vector

$$x = \left[y_{FF}\ \dot{y}_{FF}\ \psi_{FF}\ \dot{\psi}_{FF}\ y_{FR}\ \dot{y}_{FR}\ \psi_{FR}\ \dot{\psi}_{FR}\ y_{BF}\ \dot{y}_{BF}\ \psi_{BF}\ \dot{\psi}_{BF}\ y_V\ \dot{y}_V \right]^T \tag{24}$$

The primary tuning parameter for the estimation model is the Q matrix [9] that defines the uncertainty in the estimation state model, where high values for a particular state are associated with high uncertainty in the model, therefore the matrix for this estimator is defined as

$$Q = diag\left[1\,1\,1\,1\,1\,1\,1\,1\,1\,1\,1\,1\,1\,1e^9\ 1e^9\ 1e^9\ 1e^9 \right]^T \tag{25}$$

The high values in the matrix associated with equations 21 and 22 allow the filter to adapt to the creep force level required. It should be noted that tuning of this matrix is heuristic in nature and the gains associated with it will vary for data gathered in later stages of simulation and experimental testing, due to unknown noise characteristics and the model of the suspension system may not be as close to the reality as it is in simulation.

Also the KBF gains will be static in application and will have to adapt to different adhesion characteristics present on the railhead, therefore a series of tests have been undertaken for various adhesion conditions to test the efficacy of the estimator. Initially these were at static levels of adhesion at the four levels set for the study: dry; wet; low; and very low. Figure 5 shows a section of estimated creep torque data for the same track irregularity for all four of the adhesion conditions.

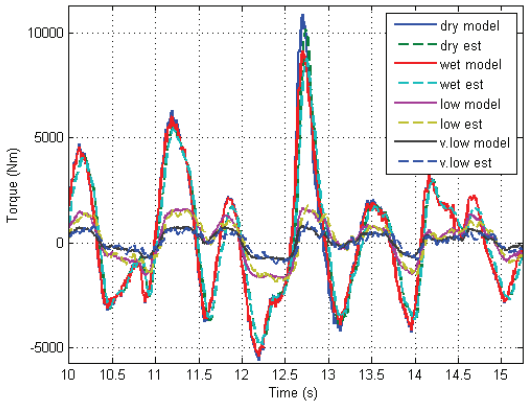

Figure 5 Creep estimations, constant adhesion

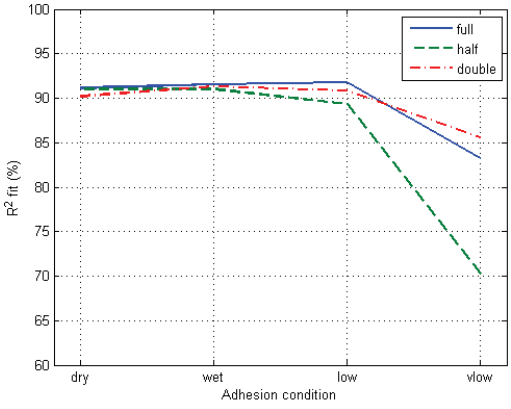

Figure 6 Estimation quality for varying excitation

Using visual inspection this shows that for all of the adhesion conditions the KBF produces a reasonable estimation of the simulated combined creep and gravitational torques. Figure 6 shows a numeric interpretation of this, using the well known coefficient of determination or R^2, [11]. Additional tests were taken at different sizes of the track irregularity, full size, half size and double size. The general trend of this plot shows that, as the adhesion level decreases to the very low level and therefore a higher proportion of the creep saturation in the simulation brings increasing nonlinearity, the estimation reduces from an average of 90% fit to around 85% fit for the full and double sized irregularities and to around 70% fit for the half sized irregularity. Therefore it shows that for full and double sized track irregularities the estimation quality is around similar values, but as the track excitation lowers so does the estimation quality, especially at the very low adhesion level.

The estimator is also expected to adapt in real time to changes in the adhesion level, and Figure 7 shows how the KBF performs. The upper graph shows the change in the adhesion level from dry to very low conditions in the period from 10 to 20 seconds, the lower graph demonstrates that the KBF adapts to this change and can still effectively estimate the creep force.

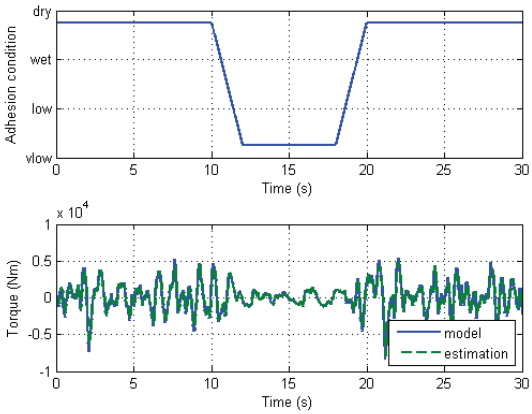

Figure 7 Varying adhesion level test

4. FURTHER TECHNIQUE DEVELOPMENT

This work is currently being expanded in a collaborative project (RSSB funded research project T959) that started in November 2010, funded by the Rail Industry Strategic research Programme with sponsorship of TSLG and VTSIC and managed by RSSB. This is primarily aimed at the use of creep force detection as a method of determining local adhesion conditions. The programme is multifaceted, including testing on a scale roller rig to determine fundamental adhesion characteristics (such as the gradients of the initial slope and the saturation levels of the creep curves), detection algorithm development, multi-bodied simulation testing and full scale testing. The authors focussed upon the development of the detection algorithm and are currently further developing the technique highlighted here along with methods of post processing the creep forces to determine adhesion levels from 'in-service' measurements. Further techniques being explored are multiple Kalman filter techniques such as [12], advanced filtering such as Particle filters [13], and the use of system identification [11].

5. CONCLUSIONS

Condition monitoring of railway vehicles is currently becoming more prevalent in the UK. This paper presents initial simulation results of the estimation of the creep forces around the wheelset, that can potentially used for many applications including adhesion level detection and wear estimation. Use is made of a full length vehicle, nonlinear plan view dynamic model and a corresponding Kalman-Bucy estimator. Results presented show initially good estimates of the creep forces and that a single linear Kalman-Bucy filter can adapt to large nonlinear adhesion changes and still produce interpretable creep force estimations.

References

[1] Bombardier, *ORBITA – predictive asset management, the future of fleet maintenance*, http://www.bombardier.com/en/transportation/, accessed 7th April 2010.

[2] C. Ward, P. Weston, E. Stewart, H. Li, R. Goodall, C. Roberts, T.X. Mei, G. Charles and R. Dixon, *Condition monitoring opportunities using vehicle based sensors*. IMechE proceedings, Part F: Rail and Rapid Transit, Vol 225, No.2/2011, pp.202-218

[3] C. Ward, R. Goodall and R. Dixon, *Contact Force Estimation in the Railway Vehicle Wheel-Rail Interface*, In Proceedings of the 18th World Congress of the International Federation of Automatic Control, Milano, 2011

[4] A.H. Wickens *Fundamentals of Rail Vehicle Dynamics, Guidance and Stability*, Swets & Zeitlinger, Lisse, Netherlands, 2003

[5] O. Polach, *Creep forces in simulations of traction vehicles running on adhesion limit*. Wear, 258(1), pp992-1000, 2005

[6] J. Kalker, *On the Rolling Contact of Two Elastic Bodies in the Presence of Dry Friction*, PhD Thesis, Delft University of Technology, Delft, Netherlands, 1967

[7] H. Harrison and T. McNanney, *Recent developments in coefficient of friction measurements at the rail/wheel interface*, Wear, 253(1), pp114-123, 2002

[8] V. Garg and R. Dukkipati, *Dynamics of Railway Vehicle Systems*, Academic press, Canada, 1984

[9] R. Kalman, *A new approach to linear filtering and prediction*. Transactions of ASME – Journal of Basic Engineering, 35-45, 1960

[10]G. Charles, R. Goodall and R. Dixon, Model-based condition monitoring at the wheel-rail interface. Vehicle System Dynamics, 46(1), 415-430, 2008

[11]L. Ljung, *System Identification, Theory for the User*, Prentice-Hall, Upper Saddle River, New Jersey, USA, 1999

[12]I. Hussain and T.X. Mei, *Multi Kalman Filtering Approach for Estimation of Wheel-Rail Contact Conditions*, In the proceedings of the UKACC International Conference on CONTROL 2010, 7-10 September, Coventry, UK

[13]B. Ristic, S. Arulampalam and N.Gordon, *Beyond the Kalman Filter, Particle Filters for Tracking Applications*, Artech House, Boston, USA, 2004

Appendix

Parameter	Dry	Wet	Low	Very Low
k_A	1.00	1.00	1.00	1.00
k_S	0.40	0.40	0.40	0.40
μ_0	0.55	0.30	0.06	0.03
A	0.40	0.40	0.40	0.40
B	0.60	0.20	0.20	0.10

Table 1 Polach model constants

Parameter	Description	Value	Units
f_{x1B}	Primary bush longitudinal damping rate	$14.012e^3$	Ns/m
f_{y1B}	Primary bush lateral damping rate	$3.503e^3$	Ns/m
f_{y2}	Secondary lateral damper rate	$59.271e^3$	Ns/m
$f_{\psi 2LIN}$	Secondary yaw damper rate (linear)	$1.9757e^6$	Ns/m
I_B	Bogie yaw inertia	2469.6	kgm^2
I_V	Vehicle yaw inertia	98784	kgm^2
I_W	Wheelset yaw inertia	721.12	kgm^2
k_{x1}	Primary longitudinal stiffness	$0.9878e^6$	N/m
k_{y1}	Primary lateral stiffness	$0.9878e^6$	N/m
k_{x1B}	Primary bush longitudinal stiffness	$14.012e^6$	N/m
k_{y1B}	Primary bush lateral stiffness	$3.503e^6$	N/m
k_{y2}	Secondary lateral stiffness	$0.237e^6$	N/m
$k_{\psi 2}$	Secondary yaw stiffness	$98.784e^3$	Nm/rad
m_B	Bogie mass	2469.6	kg
m_V	Vehicle mass	29635	kg
m_W	Wheelset mass	1106.4	kg
l	Wheelset half width	0.7452	m
L	Wheelset semi-spacing	1.3	m
D	Bush longitudinal spacing	0.8	m
c	Vehicle half length	8	m

Table 2 Vehicle model parameters